Received: 11 February 2020 | Revised: 29 September 2020 | Accepted: 1 October 2020 | Published online: 9 November 2020

DOI: 10.1002/dad2.12125

Alzheimer's & Dementia
Diagnosis, Assessment & Disease Monitoring

RESEARCH ARTICLE

Association between neurite metrics and tau/inflammatory pathology in Alzheimer's disease

Daichi Sone[1,2,3] | Yoko Shigemoto[1,3,4] | Masayo Ogawa[1] | Norihide Maikusa[1] | Kyoji Okita[1] | Harumasa Takano[1] | Koichi Kato[1] | Noriko Sato[4] | Hiroshi Matsuda[1,3]

[1] Integrative Brain Imaging Center, National Center of Neurology and Psychiatry, Tokyo, Japan

[2] Department of Clinical and Experimental Epilepsy, UCL Institute of Neurology, London, UK

[3] Cyclotron and Drug Discovery Research Center, Southern Tohoku Research Institute for Neuroscience, Fukushima, Japan

[4] Department of Radiology, National Center of Neurology and Psychiatry, Tokyo, Japan

Correspondence
Dr. Hiroshi Matsuda, National Center of Neurology and Psychiatry, 4-1-1 Ogawa-Higashi, Kodaira, Tokyo 187-8551, Japan.
Email: matsudah@ncnp.go.jp

Abstract

Introduction: The molecular mechanism of neurodegeneration, including tau and neurite complexity, is an important topic in Alzheimer's disease (AD) research.

Methods: We recruited 27 amyloid-positive individuals identified through ^{11}C-Pittsburgh compound B (PiB) positron emission tomography (PET) and 31 amyloid-negative individuals with normal cognition. All participants underwent ^{11}C-PiB and ^{18}F-THK5351 PET and magnetic resonance imaging (MRI) with neurite orientation dispersion and density imaging (NODDI) protocol. The neurite density index (NDI), orientation dispersion index (ODI), and PET images were analyzed to calculate voxel-wise correlations among the imaging modalities and correlations with cognitions.

Results: In the amyloid-positive participants, there were significant negative correlations between ^{18}F-THK5351 and NDI and between ^{18}F-THK5351 and ODI. The bilateral mesial and lateral temporal lobes were mainly involved. Regarding cognition, ^{18}F-THK5351 showed more marked associations with all cognitive domains than the other modalities.

Discussion: Tau and neuroinflammation in AD may reduce the neurite density and orientation dispersion, particularly in the mesial and lateral temporal lobes.

KEYWORDS
Alzheimer's disease, molecular imaging, neurodegeneration, neuroinflammation, orientation dispersion and density imaging, tau

1 | INTRODUCTION

Alzheimer's disease (AD), the most common neurodegenerative dementia, is pathologically characterized by senile plaques and neurofibrillary tangles consisting of amyloid beta (Aβ) and tau protein, respectively.[1] Because of the high prevalence and enormous social burden of AD,[2] efforts are being made to develop disease-modifying therapies.[3] Because the neurodegenerative process involving Aβ and tau precedes the clinical symptoms by several years,[4] the molecular mechanisms underlying the neurodegeneration are an important topic in AD research.

In vivo molecular neuroimaging with positron emission tomography (PET) is a powerful and minimally invasive tool to measure specific molecules and metabolisms in the brain. The recent development of tau PET has provided novel insight into and useful information about AD and other tauopathies.[5,6] Indeed, it has been found that tau deposition

is associated with regional gray matter loss in both AD and amyloid-negative elderly individuals.[7,8]

Meanwhile, diffusion tensor imaging (DTI) has also been applied extensively to investigate microstructures in the AD brain.[9,10] In terms of Aβ and tau pathology, for instance, DTI was reported to predict tau accumulation.[11] Recently, to address some limitations of conventional DTI, advanced diffusion MRI techniques have been demonstrated to contribute to evaluation of neurodegenerative diseases.[12] Neurite orientation dispersion and density imaging (NODDI) enables us to investigate the microstructural complexity of neurites in considerable detail,[13] and is being applied increasingly to neurological and psychiatric diseases.[14] In AD, reduced neurite density and orientation dispersion have been found in both gray and white matter.[15,16] Of interest, significant correlations between tau immunoreactivity and neurite parameters derived from NODDI were confirmed in a mouse model of tauopathy,[17] which may suggest a potential molecular mechanism of tau-related neurodegeneration involving neurite alterations. Human pathological findings also emphasize the importance of neurites in tau-related neurodegeneration.[18] However, little is known about the in vivo relationships between tau pathology and neurites in humans, which would be highly relevant to how aggregations of abnormal proteins affect neurons in the brain.

^{18}F-THK5351, one of the first-generation tau tracers,[19] exhibits distributions in tau-associated regions of AD and has favorable image contrast.[20] However, due to off-target binding to monoamine oxidase,[21] ^{18}F-THK5351 does not purely reflect tau pathology and is currently considered to target astrogliosis-related neuroinflammation as well as tau aggregation.[22] Given the key role of neuroinflammation in neurodegeneration,[23] the tracer may provide significant information on tau, neuroinflammation, and neuronal damage.

In this study, we used ^{18}F-THK5351 PET and NODDI to investigate the associations of tau and inflammatory pathology with neurite complexity in individuals with AD pathology and in amyloid-negative individuals with normal cognition. The study concept is illustrated in Supplementary Figure S1. In addition, we assessed the clinical correlations of these imaging modalities with neuropsychological measures.

HIGHLIGHTS

- We examined the association of tau and inflammation with neurite complexity in Alzheimer's disease (AD).
- Voxel-wise correlations among 18F-THK5351 positron emission tomography (PET) and neurite imaging were calculated.
- We found negative correlations of 18F-THK5351 with neurite dispersion and density.
- The bilateral mesial and lateral temporal lobes were mainly involved.
- We also reported the correlations with clinical parameters.

RESEARCH IN CONTEXT

1. Systematic review: We searched Medline and PubMed databases for studies on *in vivo* tau positron emission tomography (PET), neurite orientation dispersion and density imaging, and relevant pathological findings in Alzheimer's disease (AD). Relevant studies were additionally found in the reference lists of articles or citation lists on PubMed.
2. Interpretation: This study identified negative correlations of ^{18}F-THK5351 with both neurite dispersion and density in the AD brain, which may suggest that tau and neuroinflammatory pathology reduces the neurite density and orientation dispersion, particularly in the mesial and lateral temporal lobes. Despite the cross-sectional design, the causal relationship could be supported by the accumulated evidence on the neurotoxicity of Aβ and tau and the fact that extracellular neurofibrillary tangles are involved in abnormal neuritic clusters.
3. Future directions: Further studies using second-generation tau tracers and/or neuroinflammation-specific imaging should provide more pertinent findings. Larger sample size and longitudinal data are also desirable.

2 | METHODS

2.1 | Participants

For the AD-spectrum group (AD-S group), we recruited 27 amyloid-positive individuals (>50 years of age). Amyloid positivity was visually assessed by an independent board-certified nuclear medicine specialist from ^{11}C-Pittsburgh compound B (PiB) PET. This group included 4 preclinical patients, 7 with mild cognitive impairment, 15 with mild AD, and one with moderate AD based on Clinical Dementia Rating (CDR) scores (Table 1). To assess the molecular and neuronal relationships during disease progression, we needed individuals at various disease stages. For the healthy control (HC) group, we recruited 31 amyloid-negative individuals with normal cognition. The visual assessment of ^{11}C-PiB PET was performed by an independent board-certified nuclear medicine specialist. There were no significant differences in age, sex, or years of education between the AD-S and HC groups.

2.2 | Image acquisition

All participants underwent MRI scanning on a 3.0-T MRI system (Verio, Siemens, Erlangen, Germany). Three-dimensional sagittal

TABLE 1 Demographics of the AD-S and HC groups in this study

	AD-S group (n = 27)	HC group (n = 31)	*P*
Age, y (mean ± SD)	72.2 ± 8.4	69.0 ± 7.0	0.124
Sex (F:M)	17:10	17:14	0.531
Education, y (mean ± SD)	13.7 ± 2.4	14.0 ± 3.0	0.645
CDR	0, 4; 0.5, 7; 1.0, 15; 2.0, 1	all 0	<0.001
MMSE (mean ± SD)	23.3 ± 4.5	29.2 ± 1.1	<0.001
MoCA (mean ± SD)	20.0 ± 5.8	27.3 ± 2.2	<0.001
WMS-R LM-II (mean ± SD)	4.5 ± 5.0	12.6 ± 3.9	<0.001
SUVR of ^{11}C-PiB within whole cortex (mean ± SD)	2.03 ± 0.75	0.89 ± 0.07	<0.001

Abbreviations: AD-S, Alzheimer's disease spectrum; CDR, Clinical Dementia Rating; HC, healthy controls; MMSE, Mini-Mental State Examination; MoCA, Montreal Cognitive Assessment; SUVR, standardized uptake value ratio; WMS-R LM-II, Wechsler Memory Scale Logical Memory II.

T1-weighted magnetization prepared rapid acquisition with gradient echo (MPRAGE) images were obtained as follows: repetition time (TR)/echo time (TE), 1900 ms/2.52 ms; flip angle (FA), 9°; in-plane resolution, 1.0 × 1.0 mm; 1.0-mm effective slice thickness with no gap; 300 slices; matrix, 256 × 256; field of view (FOV), 25 × 25 cm. For the diffusion imaging, a multi-shell protocol was acquired along 30 non-collinear directions at two b-values (1000 and 2000 s/mm^2), as well as two images with reversed phase encoding (blip up/down) without any diffusion gradient. The diffusion MRI parameters were as follows: TR/TE, 17700 ms/93 ms; FA, 90°; in-plane resolution, 2.0 × 2.0 mm; 2.0-mm effective slice thickness; 74 slices; matrix, 114 × 114; FOV, 22.4 × 22.4 cm.

All PET/computed tomography (CT) scans were performed on a Siemens/Biograph 16 scanner (3D acquisition mode; 81 image planes; 16.2-cm axial FOV; 4.2-mm transaxial resolution; 4.7-mm axial resolution; 2-mm slice interval). A low-dose CT scan was performed for attenuation correction. For ^{11}C-PiB imaging, ^{11}C-PiB at a dose of 555 MBq was injected intravenously 50 minutes before the PET/CT scan; the emission scan duration was 20 minutes. For ^{18}F-THK5351 imaging, ^{18}F-THK5351 at a dose of 185 MBq was injected 40 minutes before the scan; the scan duration was 20 minutes. PET/CT images were reconstructed using a combination of Fourier rebinning and Ordered Subsets Expectation Maximization. The average interval between the ^{11}C-PiB, ^{18}F-THK5351, and MRI was 12.3 ± 13.7 days.

2.3 | PET processing

After partial volume correction with the PETPVE12 toolbox,[24] the ^{11}C-PiB and ^{18}F-THK5351 PET images were normalized using Statistical Parametric Mapping 12 software (SPM12; http://www.fil.ion.ucl.ac.uk/spm/). The participants' PET images were coregistered to their T1-weighted images and normalized to the Montreal Neurological Institute (MNI) space with the Diffeomorphic Anatomical Registration Through Exponentiated Lie (DARTEL) method.[25] After spatial normalization, all of the PET images were divided by the individual's positive mean uptake value of cerebellar gray matter, and finally the standardized uptake value ratio (SUVR) images were obtained. Each SUVR of PET image was smoothed by an 8-mm full-width at half-maximum (FWHM) Gaussian kernel.

2.4 | Diffusion MRI processing

The diffusion MRI data were preprocessed by topup correction for geometrical distortions and eddy current and motion correction by eddy using FMRIB Software Library (FSL), version 5.0.11.[26] Subsequently, the NODDI model was fitted using the NODDI toolbox (https://www.nitrc.org/projects/noddi_toolbox/) running on MATLAB (MathWorks, Natick, MA, USA), and then the neurite density index (NDI) and orientation dispersion index (ODI) maps were calculated. These images were also coregistered to the T1-weighted images and normalized to the MNI space with DARTEL. When analyzing the PET images, we focused on gray matter. Therefore, the normalized NODDI images were masked by a gray matter image derived from the SPM template. Finally, smoothing was performed with an 8-mm FWHM Gaussian kernel. To avoid the potential noise from cerebrospinal fluid, we visually checked the masking out with careful attention.

2.5 | Voxel-wise correlations between PET and NODDI

To estimate relationships between PET and NODDI, we used the VoxelStats toolbox.[27] Using a general linear model, the toolbox calculated voxel-wise correlations between two imaging modalities with age, sex, and education years as covariates. We analyzed the correlations for all combinations of PET- and NODDI-related imaging modalities, namely, ^{11}C-PiB, ^{18}F-THK5351, NDI, and ODI. In addition, to reflect the pathological processes in AD, these analyses were performed separately in the AD-S group and the HC group. BrainNet Viewer (http://www.nitrc.org/projects/bnv/) was used to visualize the results.[28]

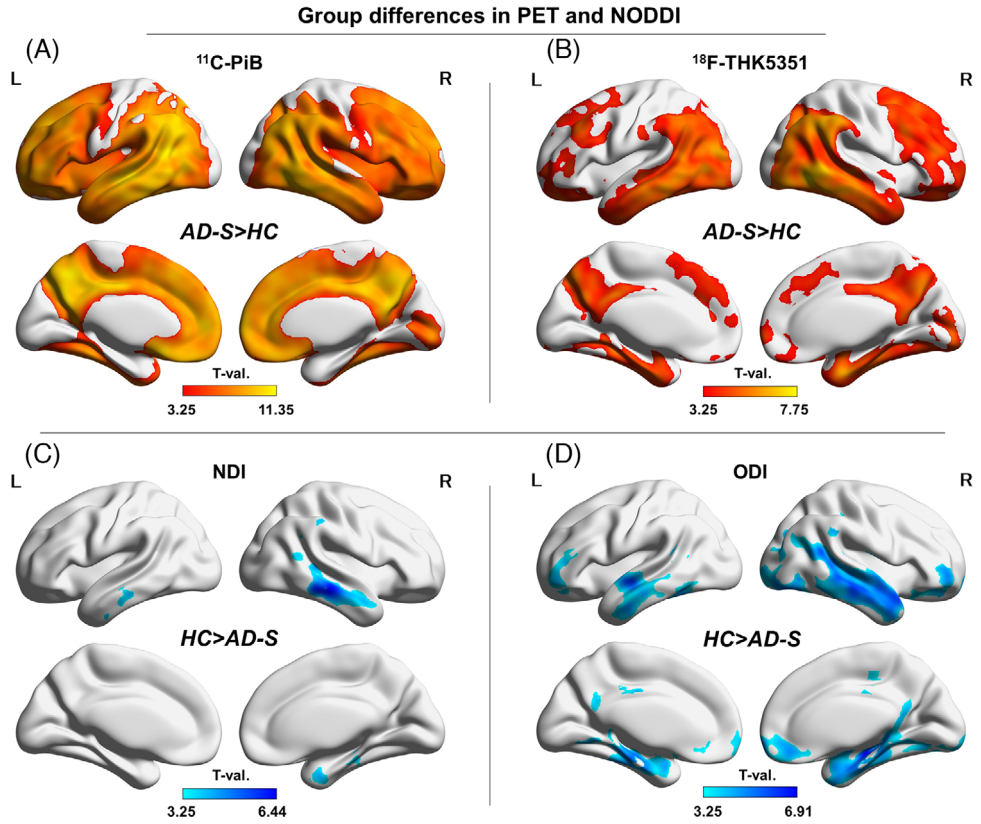

FIGURE 1 Group differences between the AD-S and HC groups. (A) ^{11}C-PiB, (B) ^{18}F-THK5351, (C) the NDI, and (D) the ODI. Color bars denote the statistically significant T-values from minimum to maximum

2.6 | Neuropsychological assessments

All participants underwent the Mini-Mental State Examination (MMSE), Montreal Cognitive Assessment (MoCA), and Wechsler Memory Scale-revised Logical Memory II (WMS-R LM-II). For correlation analysis between imaging and cognition, we used WMS-R LM-II as a measure of delayed recall, the execution domain of the MoCA for executive function, and the orientation domain of the MoCA for orientation function. These analyses were also performed separately in each AD-S and HC group.

2.7 | Statistics

To compare clinical demographics between the AD-S and HC groups, we used an unpaired *t* test for continuous variables and Pearson chi-square test for categorical parameters in SPSS software, version 25.0 (SPSS Japan, Tokyo, Japan). A *P*-value less than 0.05 was deemed statistically significant.

For whole-brain SPM12 analyses, that is, group comparison and correlation analysis with neuropsychological scores, we used a two-sample *t* test and multiple regression designs, respectively, with age, sex, and education years as covariates. Results with the following criteria were deemed significant: a height threshold of $P < 0.001$ (uncorrected) and an extent threshold of $P < 0.05$ (family-wise error [FWE] corrected).

For correlations between different imaging modalities, VoxelStats generated the results based on random field theory (RFT) correction.[27] The significance level was set at $P < 0.001$ (RFT-corrected).

To interpret the strength and the fit of the relationships, we also included the box or scatter plots of mean values of PET or NODDI within the significant areas in each analysis (Supplementary Figure S2).

2.8 | Standard protocol approvals, registrations, and patient consents

All participants provided written informed consent before participation. This cross-sectional observational study has been approved by the institutional review board at the National Center of Neurology and Psychiatry Hospital.

3 | RESULTS

3.1 | Group differences in PET and NODDI

Figure 1 and Supplementary Figure S2-A show the group difference results. Both ^{11}C-PiB and ^{18}F-THK5351 showed significant and

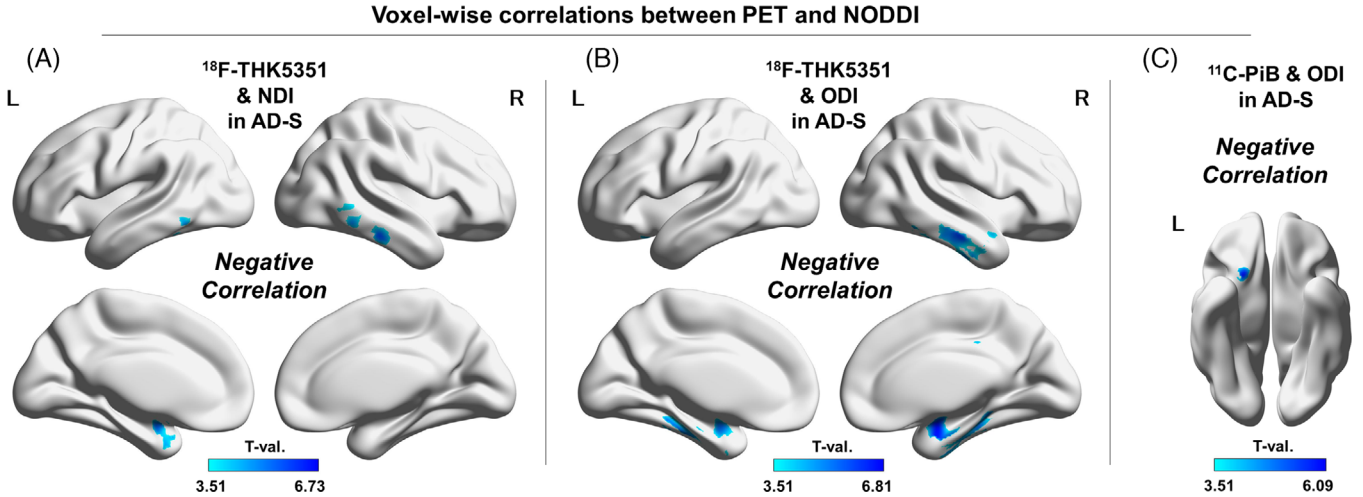

FIGURE 2 Voxel-wise correlations between PET and NODDI. (A) Negative correlations between ^{18}F-THK5351 and the NDI in the AD-S group, (B) negative correlations between ^{18}F-THK5351 and the ODI in the AD-S group, and (C) negative correlations between ^{11}C-PiB and the ODI in the AD-S group. Color bars denote the statistically significant T-values from minimum to maximum

widespread increases in the AD-S group (Figure 1-A and B). In addition, whereas the NDI was decreased mainly in the bilateral temporal lobes in the AD-S group (Figure 1-C), the ODI was reduced in orbitofrontal areas and the cingulate gyri, in addition to the temporal lobes (Figure 1-D).

3.2 | Image correlations between PET and NODDI

The AD-S group showed significant negative correlations between ^{18}F-THK5351 and the NDI (Figure 2-A) and between ^{18}F-THK5351 and the ODI (Figure 2-B). The bilateral temporal lobes showed more significant associations, although the right posterior cingulate gyrus was also correlated between ^{18}F-THK5351 and the ODI (Figure 2-B). In addition, there was a small negative correlation in the left orbitofrontal cortex between ^{11}C-PiB and the ODI (Figure 2-C).

There were widespread positive correlations between ^{11}C-PiB and ^{18}F-THK5351 in the cortex in the AD-S group (Figure 3-A), although a more restricted area showed the same correlations in the HC group (Figure 3-C). The NDI and ODI also showed positive correlations in the AD-S group (Figure 3-B), but the same correlations were much more widely found in the HC group (Figure 3-D).

The numerical relationships can be found in Supplementary Figures S2-B and C. The other undescribed analyses in Figures 2 and 3 were not significant, and the list of them is shown in Supplementary Table S1.

3.3 | Correlations with neuropsychological measurements

Significant correlations with cognitive functions were found only in the AD-S group, and the other unillustrated analyses in Figures 4 and 5 were not significant. The list of insignificant analyses can be found in Supplementary Table S1. In additionally, Supplementary Figure S2 (D-F) presents the numerical correlations.

With delayed recall, both ^{11}C-PiB and ^{18}F-THK5351 showed negative correlations in the cortex, with the latter showing a greater and broader association (Figure 4-A, B). In addition, the ODI was also positively correlated with delayed recall in the bilateral posterior cingulate gyri (Figure 4-C).

The right mesial temporal lobe was negatively associated with orientation in ^{18}F-THK5351, the NDI, and the ODI (Figure 4-D–F), whereas ^{11}C-PiB showed no significant correlations. In addition, ^{18}F-THK5351 presented significant negative correlations with orientation in the bilateral mesial and lateral temporal lobes, cingulate gyri, and orbitofrontal cortices (Figure 4-D).

Finally, the right posterior cingulate gyrus was correlated with executive function in all modalities (negatively in PET and positively in NODDI) (Figure 5-A–D). In addition, the bilateral frontal lobes and lateral parietal lobes were also negatively correlated with executive function in ^{11}C-PiB and ^{18}F-THK5351 (Figure 5-A, B).

4 | DISCUSSION

In this study, we first examined the voxel-wise imaging correlations among ^{11}C-PiB, ^{18}F-THK5351, and NODDI in individuals with AD pathology and in amyloid-negative individuals with normal cognition. We found negative correlations of ^{18}F-THK5351 with the NDI and ODI in the AD-S group, mainly in the bilateral temporal lobes. This finding suggests that tau aggregation and the neuroinflammatory processes of these regions may reduce neurite density and dispersion in AD. It was also indicated that Aβ deposition in the left orbitofrontal cortex is associated with decreased neurite orientation dispersion. Although this cross-sectional study cannot determine causal relationships by design,

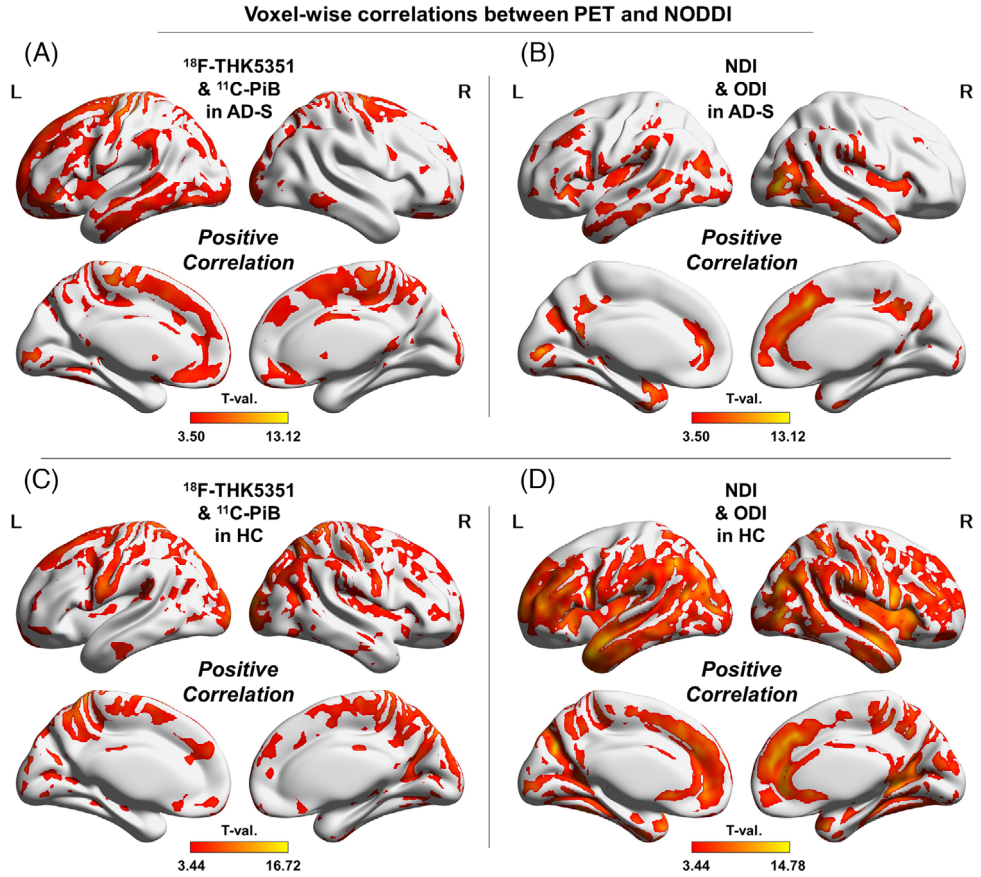

FIGURE 3 Voxel-wise correlations between PET and NODDI. (A) Positive correlations between ^{18}F-THK5351 and ^{11}C-PiB in the AD-S group, (B) positive correlations between the NDI and ODI in the AD-S group, (C) positive correlations between ^{18}F-THK5351 and ^{11}C-PiB in the HC group, and (D) positive correlations between the NDI and ODI in the HC group. Color bars denote the statistically significant T-values from minimum to maximum

this relationship should be supported by the accumulated evidence on the neurotoxicity of Aβ and tau.[29,30]

According to the hallmark pathological theory of AD,[1,31] neurofibrillary tangles first target extrahippocampal temporal cortices and then damage the hippocampus through the perforant pathway. Thus the lateral and mesial temporal lobes, where we found a significant association between ^{18}F-THK5351 and neurites (Figure 2-A and B), would be the areas most affected by tau. Aβ accumulates primarily in neocortices and is less associated with AD progression and cognitive impairment.[1,32,33] A key role of tau is supposed to lie in mediating the Aβ toxicity at post-synapse.[29,30] Accordingly, the relationship between tau and dendrites may have a significant impact on neurodegeneration in AD. Of interest, dystrophic neurites are pathologically associated with both Aβ and tau,[18] and extracellular neurofibrillary tangles are involved in abnormal neuritic clusters.[34] We found a broader correlation of ^{18}F-THK5351 with the ODI than with the NDI in the posterior cingulate gyrus and in the temporal lobes, and AD-related dystrophic neurites may thus be more associated with orientation dispersion changes. In fact, NODDI parameters were reported to show a good agreement with myelin or neuronal density in histopathology[35] as well as to be associated with microglial alterations.[36] Thus it would be reasonable to link NODDI abnormalities with neuroinflammatory process.

In addition, we found a significant positive correlation between ^{11}C-PiB and ^{18}F-THK5351, even in visually amyloid-negative individuals (Figure 3-C), although the AD-S group showed much broader correlations (Figure 3-A). Possibly, even in brains with visually normal ^{11}C-PiB, subtle amyloid deposition might have occurred and might be correlated with tau and inflammatory pathology. However, it should be noted that neither ^{11}C-PiB nor ^{18}F-THK5351 was related to neurite parameters in this group. On the other hand, the correlation between NODDI parameters, namely, the NDI and ODI, was much stronger and broader in the HC group (Figure 2-D) than in the AD-S group (Figure 2-B). This finding suggests that AD-related pathology may widely destroy the relationship of neurite density and dispersion that can be seen in healthy elderly people.

In addition, we investigated associations with neuropsychological measures, specifically delayed recall, executive function, and orientation. Overall, among the imaging modalities in the AD-S group, ^{18}F-THK5351 showed the strongest and broadest correlations with all scores, which is consistent with the past literature concerning tau PET.[33] It is notable that a reduced ODI was correlated with worsening

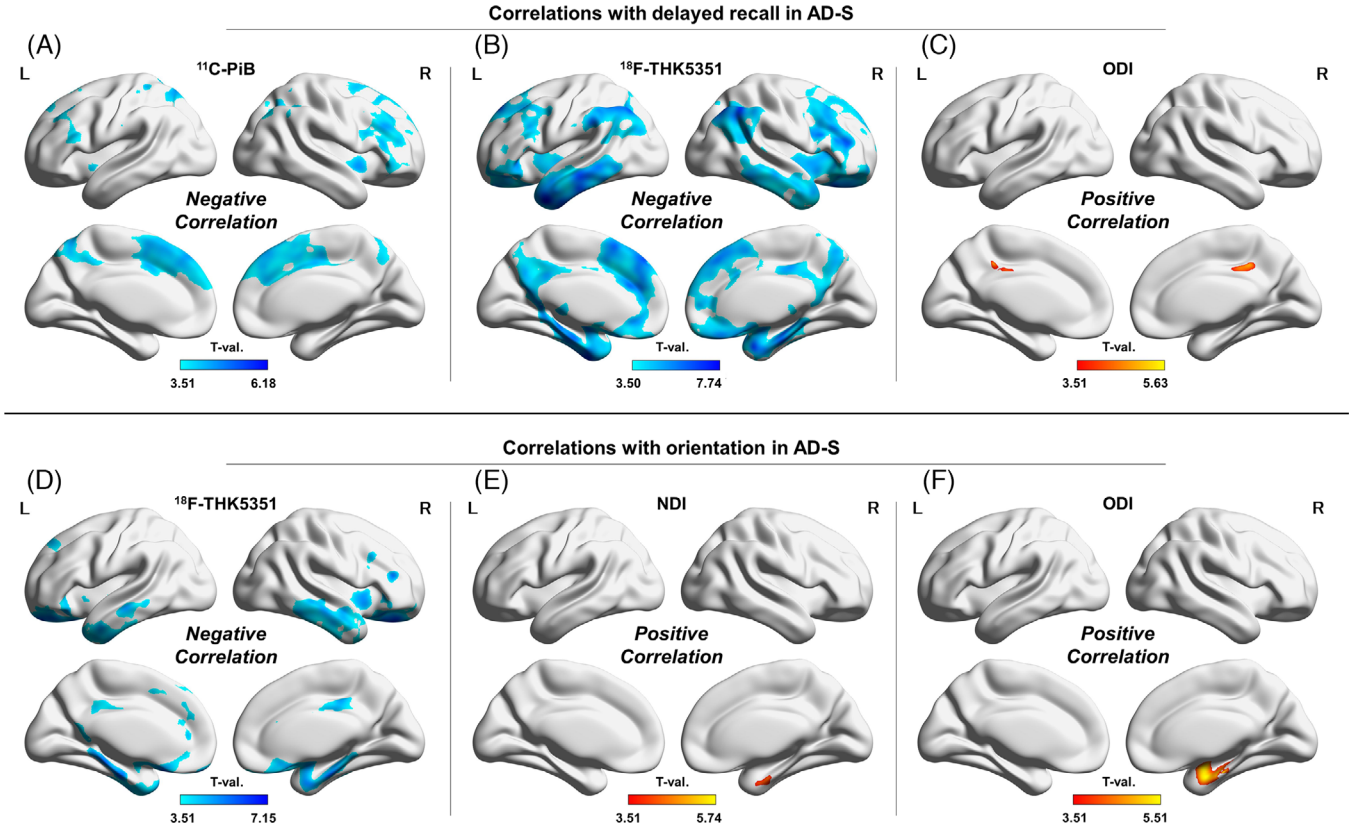

FIGURE 4 Correlations with delayed recall (A-C) and orientation (D-F) in the AD-S group. (A) ^{11}C-PiB, (B) ^{18}F-THK5351, and (C) the ODI with delayed recall. (D) ^{18}F-THK5351, (E) the NDI, and (F) the ODI with orientation. Color bars denote the statistically significant T-values from minimum to maximum

of delayed recall in the posterior cingulate gyri (Figure 4-C), where significant correlations were observed between ^{18}F-THK5351 and ODI (Figure 2-B). Considering this relationship, tau and inflammatory pathology in these areas may affect amnestic symptoms by reducing neurite dispersions in AD. In addition, the areas correlated with executive function were mainly the frontoparietal cortices (Figure 5). According to a functional MRI study of dementia,[37] executive tasks activate fronto-parieto-occipital networks in both AD and healthy elderly individuals but require greater activation of the brain in AD.[37] In particular, the burden of Aβ, tau, and neuroinflammation may cause dysfunction in these areas (Figure 5-A, B) and impaired execution in AD, whereas the right posterior cingulate gyrus might play a significant role in terms of neurites (Figure 5-C, D). Regarding disorientation, the bilateral posterior cingulate gyri and right middle temporal gyrus are supposed to be potential neural correlates,[38,39] which is consistent with the areas showing correlations on ^{18}F-THK5351 (Figure 4-D). Finally, there was no correlation in the HC group, which could be attributed to the lower accumulation of Aβ and tau or the ceiling effect of the examination scores.

In the field of diffusion MRI research on AD, DTI has been widely used and demonstrated relevant findings, including axonal damages, an important role of fornix, and network disruption.[9,10] Of interest, a longitudinal study reported the association between diffusivity in the hippocampal cingulum bundle and tau accumulation.[11] Our results using NODDI, which may have more specific characterization of the tissue microstructure,[12] could provide further insights into the relationships between tau pathology and microstructures estimated by diffusion MRI.

Most of previous studies of NODDI findings in AD have focused on white matter changes,[15,40,41] or specific regions of the cortex.[16] These studies reported reductions in both the NDI and ODI in regions related to AD,[15,16,40,41] and NDI in several cortical areas showed positive correlations with the MMSE,[16] which is compatible with the present results (Figure 1-C, D and Figures 4–5). A more recent study revealed broader reduction of the NDI and ODI mainly in bilateral temporal lobes in AD.[42] Our NODDI findings in the gray matter are generally consistent with the previous report and may extend the understanding of correlation analysis with specific neuropsychological domains. A potentially different mechanism in memory between individuals with and without the ε4 allele of the apolipoprotein E (*APOE*) gene was also suggested in another recent article using NODDI.[43] However, the group differences and neuropsychological correlations of NODDI were generally less marked than those of ^{18}F-THK5351, and NODDI might not currently be a comparable biomarker to tau-related PET for the diagnosis or disease monitoring of AD.

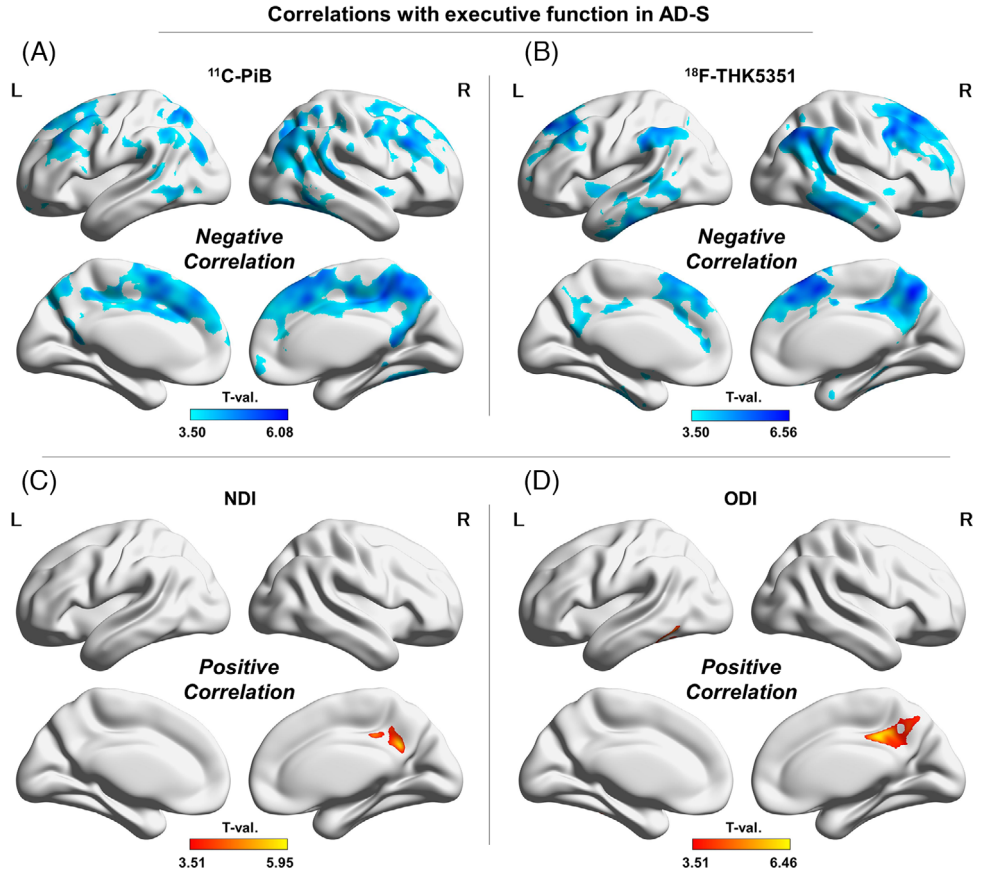

FIGURE 5 Correlations with executive function in the AD-S group. (A) ^{11}C-PiB, (B) ^{18}F-THK5351, (C) the NDI, and (D) the ODI. Color bars denote the statistically significant T-values from minimum to maximum

This study has several limitations. First, the sample size was relatively small, and the use of uncorrected *P* values for the height threshold in SPM should also be kept in mind. However, we believe that the extent threshold with FWE correction would overcome this issue, and our findings may thus provide novel insights into AD. Second, although ^{18}F-THK5351 is considered to reflect the combined pathology of tau and astrogliosis-related inflammation,[22] we were unable to evaluate these two mechanisms separately. Further studies using second-generation tau tracers and/or neuroinflammation-specific imaging should provide more pertinent findings.

Finally, the potential partial volume effect on diffusion MRI has to be addressed carefully.[44] Accordingly, we corrected the correlations of ^{18}F-THK5351 with NDI and ODI (Figure 2-A and B), which were the main findings in this study, for cortical thickness calculated by Computational Anatomy Toolbox (CAT12) (Supplementary Figure S3). In the partial correlation analyses with cortical thickness of the right inferior temporal gyrus as a covariate, the results with both NDI and ODI remained significant (partial correlation coefficient $r = -0.679$ and -0.716, respectively, both $P < 0.001$). Although we mainly applied voxel-wise methods to explore the whole cerebral gray matters including subcortical structures such as hippocampus, the limitation of potential confounding by partial volume effect should be kept in mind for careful interpretation.

5 | CONCLUSION

This study identified negative correlations of ^{18}F-THK5351 with the NDI and ODI in the AD-S brain, which may suggest that tau and neuroinflammatory pathology reduces the neurite density and orientation dispersion, particularly in the mesial and lateral temporal lobes. Combined with clinical correlation results, these findings extend our knowledge of neurodegenerative mechanisms and cognition.

ACKNOWLEDGMENTS

This study was supported by the following funding: the Brain Mapping by Integrated Neurotechnologies for Disease Studies (Brain/MINDS) project (grant no. 18dm0207017h0005) from the Japan Agency for Medical Research and Development (AMED).

CONFLICT OF INTEREST

None declared.

DATA AVAILABILITY STATEMENT

Data not included in the article will be made available to qualified researchers on reasonable request subject to ethics approval.

ORCID

Daichi Sone https://orcid.org/0000-0001-9617-706X

REFERENCES

1. Braak H, Braak E. Neuropathological stageing of Alzheimer-related changes. *Acta Neuropathol*. 1991;82:239-259.
2. Alzheimer's Association. 2019 Alzheimer's disease facts and figures. *Alzheimers Dement*. 2019;15:321-387.
3. Long JM, Holtzman DM. Alzheimer disease: an update on pathobiology and treatment strategies. *Cell*. 2019;179:312-339.
4. Jack CR Jr, Knopman DS, Jagust WJ, et al. Hypothetical model of dynamic biomarkers of the Alzheimer's pathological cascade. *Lancet Neurol*. 2010;9:119-128.
5. Matsuda H, Shigemoto Y, Sato N. Neuroimaging of Alzheimer's disease: focus on amyloid and tau PET. *Jpn J Radiol*. 2019;37:735-749.
6. Leuzy A, Chiotis K, Lemoine L, et al. Tau PET imaging in neurodegenerative tauopathies-still a challenge. *Mol Psychiatry*. 2019;24:1112-1134.
7. Sone D, Imabayashi E, Maikusa N, et al. Regional tau deposition and subregion atrophy of medial temporal structures in early Alzheimer's disease: a combined positron emission tomography/magnetic resonance imaging study. *Alzheimers Dement (Amst)*. 2017;9:35-40.
8. Shigemoto Y, Sone D, Ota M, et al. Voxel-based correlation of (18)F-THK5351 accumulation and gray matter volume in the brain of cognitively normal older adults. *EJNMMI Res*. 2019;9:81.
9. Acosta-Cabronero J, Nestor PJ. Diffusion tensor imaging in Alzheimer's disease: insights into the limbic-diencephalic network and methodological considerations. *Front Aging Neurosci*. 2014;6:266.
10. Amlien IK, Fjell AM. Diffusion tensor imaging of white matter degeneration in Alzheimer's disease and mild cognitive impairment. *Neuroscience*. 2014;276:206-215.
11. Jacobs HIL, Hedden T, Schultz AP, et al. Structural tract alterations predict downstream tau accumulation in amyloid-positive older individuals. *Nat Neurosci*. 2018;21:424-431.
12. Andica C, Kamagata K, Hatano T. MR biomarkers of degenerative brain disorders derived from diffusion imaging. *J Magn Reson Imaging*. 2019.
13. Zhang H, Schneider T, Wheeler-Kingshott CA, Alexander DC. NODDI: practical in vivo neurite orientation dispersion and density imaging of the human brain. *Neuroimage*. 2012;61:1000-1016.
14. Sone D. Neurite orientation and dispersion density imaging: clinical utility, efficacy, and role in therapy. *Rep Med Imaging*. 2019;12:17-29.
15. Slattery CF, Zhang J, Paterson RW, et al. ApoE influences regional white-matter axonal density loss in Alzheimer's disease. *Neurobiol Aging*. 2017;57:8-17.
16. Parker TD, Slattery CF, Zhang J, et al. Cortical microstructure in young onset Alzheimer's disease using neurite orientation dispersion and density imaging. *Hum Brain Mapp*. 2018;39:3005-3017.
17. Colgan N, Siow B, O'Callaghan JM, et al. Application of neurite orientation dispersion and density imaging (NODDI) to a tau pathology model of Alzheimer's disease. *Neuroimage*. 2016;125:739-744.
18. Duyckaerts C, Delatour B, Potier MC. Classification and basic pathology of Alzheimer disease. *Acta Neuropathol*. 2009;118:5-36.
19. Chandra A, Valkimadi PE, Pagano G, et al. Applications of amyloid, tau, and neuroinflammation PET imaging to Alzheimer's disease and mild cognitive impairment. *Hum Brain Mapp*. 2019;40:5424-5442.
20. Betthauser TJ, Lao PJ, Murali D, et al. In Vivo Comparison of Tau Radioligands (18)F-THK-5351 and (18)F-THK-5317. *J Nucl Med*. 2017;58:996-1002.
21. Ng KP, Pascoal TA, Mathotaarachchi S, et al. Monoamine oxidase B inhibitor, selegiline, reduces 18F-THK5351 uptake in the human brain. *Alzheimers Res Ther*. 2017;9:25.
22. Okamura N, Harada R, Ishiki A, Kikuchi A, Nakamura T, Kudo Y. The development and validation of tau PET tracers: current status and future directions. *Clin Transl Imaging*. 2018;6:305-316.
23. Calsolaro V, Edison P. Neuroinflammation in Alzheimer's disease: current evidence and future directions. *Alzheimers Dement*. 2016;12:719-732.
24. Gonzalez-Escamilla G, Lange C, Teipel S, Buchert R, Grothe MJ. PETPVE12: an SPM toolbox for partial volume effects correction in brain PET - Application to amyloid imaging with AV45-PET. *Neuroimage*. 2017;147:669-677.
25. Ashburner J. A fast diffeomorphic image registration algorithm. *Neuroimage*. 2007;38:95-113.
26. Smith SM, Jenkinson M, Johansen-Berg H, et al. Tract-based spatial statistics: voxelwise analysis of multi-subject diffusion data. *Neuroimage*. 2006;31:1487-1505.
27. Mathotaarachchi S, Wang S, Shin M, et al. VoxelStats: a MATLAB package for multi-modal voxel-wise brain image analysis. *Front Neuroinform*. 2016;10:20.
28. Xia M, Wang J, He Y. BrainNet Viewer: a network visualization tool for human brain connectomics. *PLoS One*. 2013;8:e68910.
29. Ittner LM, Ke YD, Delerue F, et al. Dendritic function of tau mediates amyloid-beta toxicity in Alzheimer's disease mouse models. *Cell*. 2010;142:387-397.
30. Ittner A, Ittner LM. Dendritic tau in Alzheimer's disease. *Neuron*. 2018;99:13-27.
31. Braak H, Braak E, Bohl J. Staging of Alzheimer-related cortical destruction. *Eur Neurol*. 1993;33:403-408.
32. Giannakopoulos P, Herrmann FR, Bussiere T, et al. Tangle and neuron numbers, but not amyloid load, predict cognitive status in Alzheimer's disease. *Neurology*. 2003;60:1495-1500.
33. Ossenkoppele R, Schonhaut DR, Scholl M, et al. Tau PET patterns mirror clinical and neuroanatomical variability in Alzheimer's disease. *Brain*. 2016;139:1551-1567.
34. Munoz DG, Wang D. Tangle-associated neuritic clusters. A new lesion in Alzheimer's disease and aging suggests that aggregates of dystrophic neurites are not necessarily associated with beta/A4. *Am J Pathol*. 1992;140:1167-1178.
35. Wang N, Zhang J, Cofer G, et al. Neurite orientation dispersion and density imaging of mouse brain microstructure. *Brain Struct Funct*. 2019;224:1797-1813.
36. Yi SY, Stowe NA, Barnett BR, Dodd K, Yu JJ. Microglial density alters measures of axonal integrity and structural connectivity. *Biol Psychiatry Cogn Neurosci Neuroimaging*. 2020;S2451-9022(20):30102-30106.
37. Firbank M, Kobeleva X, Cherry G, et al. Neural correlates of attention-executive dysfunction in lewy body dementia and Alzheimer's disease. *Hum Brain Mapp*. 2016;37:1254-1270.
38. Hirono N, Mori E, Ishii K, et al. Hypofunction in the posterior cingulate gyrus correlates with disorientation for time and place in Alzheimer's disease. *J Neurol Neurosurg Psychiatry*. 1998;64:552-554.
39. Yamashita KI, Uehara T, Prawiroharjo P, et al. Functional connectivity change between posterior cingulate cortex and ventral attention network relates to the impairment of orientation for time in Alzheimer's disease patients. *Brain Imaging Behav*. 2019;13:154-161.
40. Fu X, Shrestha S, Sun M, et al. Microstructural white matter alterations in mild cognitive impairment and Alzheimer's disease : study based on Neurite Orientation Dispersion and Density Imaging (NODDI). *Clin Neuroradiol*. 2020;30(3):569-579.
41. Wen Q, Mustafi SM, Li J, et al. White matter alterations in early-stage Alzheimer's disease: a tract-specific study. *Alzheimers Dement (Amst)*. 2019;11:576-587.

42. Vogt NM, Hunt JF, Adluru N, et al. Cortical microstructural alterations in mild cognitive impairment and Alzheimer's disease dementia. *Cereb Cortex*. 2020;30:2948-2960.
43. Evans SL, Dowell NG, Prowse F, Tabet N, King SL, Rusted JM. Mid age APOE epsilon4 carriers show memory-related functional differences and disrupted structure-function relationships in hippocampal regions. *Sci Rep*. 2020;10:3110.
44. Henf J, Grothe MJ, Brueggen K, Teipel S, Dyrba M. Mean diffusivity in cortical gray matter in Alzheimer's disease: the importance of partial volume correction. *Neuroimage Clin*. 2018;17:579-586.

SUPPORTING INFORMATION

Additional supporting information may be found online in the Supporting Information section at the end of the article.

How to cite this article: Sone D Shigemoto Y, Ogawa M, et al. Association between neurite metrics and tau/inflammatory pathology in Alzheimer's disease. *Alzheimer's Dement*. 2020;12:e12125. https://doi.org/10.1002/dad2.12125